European Journal of Radiology 118 (2019) 251–256

Contents lists available at ScienceDirect

European Journal of Radiology

journal homepage: www.elsevier.com/locate/ejrad

Research article

Prognostic and predictive value of histogram analysis in patients with non-small cell lung cancer refractory to platinum treated by nivolumab: A multicentre retrospective study

Marco Ravanelli[a], Giorgio Maria Agazzi[a,*], Gianluca Milanese[b], Elisa Roca[c], Mario Silva[b], Marcello Tiseo[d], Paolo Rondi[c], Alice Baggi[c], Balaji Ganeshan[e], Margherita Muri[f], Stefano Panni[g], Camilla Botti[a], Nicola Sverzellati[b], Roberto Maroldi[a], Alfredo Berruti[c], Davide Farina[a]

[a] University of Brescia, Department of Radiology, P.le Spedali Civili 1, 25123, Brescia, Italy
[b] University of Parma, Department of Radiology, via Università, 12, I 43121, Parma, Italy
[c] University of Brescia, Department of Oncology, P.le Spedali Civili 1, 25123, Brescia, Italy
[d] Department of Medicine and Surgery, University of Parma and Medical Oncology Unit, University Hospital of Parma, Italy
[e] University College London, Institute of Nuclear Medicine, Gower Street, London, United Kingdom
[f] ASST Cremona, Department of Radiology, Viale Concordia n 1, 26100, Cremona, Italy
[g] ASST Cremona, Department of Oncology Italy

ARTICLE INFO

Keywords:
Tomography, X-Ray computed
Neoplasms/diagnostic imaging
Nivolumab
Lung neoplasms
Immunotherapy
Histogram analysis, iRECIST

ABSTRACT

Purpose: The aim of this study was to assess computed-tomography histogram analysis (CTHA) as prognostic and predictive factor in platinum-refractory non-small cell lung carcinoma (NSCLC) treated with immune checkpoint inhibitor Nivolumab.

Method: One hundred and four patients were enrolled from 3 different centers. CT was performed using similar parameters among different scanners. CTHA was performed with the proprietary software TexRAD, which extracts histogram features at different spatial scale (spatial scale filters, SSF) producing 30 CTHA features per patients. Cross-validated Least Absolute Shrinkage and Selection Operator LASSO was used to select those features which were related to overall and progression-free survival (OS and PFS, respectively). High- and low-risk subgroups were identified using the best cutoff.

Results: Median follow-up was 13.8 weeks. Median OS and PFS were 7.3 and 3 months, respectively. LASSO selected kurtosis obtained by SSF = 4 mm as the single feature related to OS, leading to an hazard ratio (HR) of 0.476 (95%CI 0.29-0.77). PFS was related with kurtosis SSF = 6 mm, with HR of 0.556 (95%CI 0.36-0.86).

Conclusion: Despite its limitations, this study is the first which suggests that CTHA could play a role in stratifying prognosis and treatment response in patients with NSCLC treated with Nivolumab.

1. Introduction

Lung cancer is one of the most lethal and frequent types of cancer worldwide, with an average 5-year overall survival rate stable at around 15% [1]. Improved understanding of the immune system and its role in limiting cancer proliferation has afforded comprehensive opportunities for novel therapeutic approaches [2]. Indeed, immunotherapy by immune checkpoint inhibitors has led to impressive advances in oncologic outcome, including lung cancer management in clinical practice. In particular, PD-1/PDL-1 inhibitors play a leading

Abbreviations: CECT, contrast-enhanced CT; CTCAE, common terminology criteria for adverse Events; CTHA, CT histogram analysis; ECOG, eastern cooperative oncology group; HR, hazard ratio; ICC, intraclass correlation coefficient; LASSO, least absolute shrinkage and selection operator; NSCLC, non-small cell lung cancer; OS, overall survival; PACS, picture archiving and communication systems; PFS, progression-free survival; SSF, spatial scale filter; TKI, tyrosine kinase inhibitor

* Corresponding author.
E-mail addresses: marcoravanelli@hotmail.it (M. Ravanelli), giorgiomaria.agazzi@gmail.com (G.M. Agazzi), gianluca.milanese@studenti.unipr.it (G. Milanese), elisaroca@gmail.com (E. Roca), mario.silva@unipr.it (M. Silva), mtiseo@ao.pr.it (M. Tiseo), paolo.rondi92@gmail.com (P. Rondi), a.baggi001@studenti.unibs.it (A. Baggi), b.ganeshan@ucl.ac.uk (B. Ganeshan), margheritamuri@gmail.com (M. Muri), stefanopanni@alice.it (S. Panni), botti.camilla@gmail.com (C. Botti), nicola.sverzellati@unipr.it (N. Sverzellati), roberto.maroldi@unibs.it (R. Maroldi), alfredo.berruti@unibs.it (A. Berruti), davide.farina@unibs.it (D. Farina).

https://doi.org/10.1016/j.ejrad.2019.07.019
Received 26 March 2019; Received in revised form 24 May 2019; Accepted 16 July 2019

role and act by adaptive immune suppression within the tumor, resulting in immune checkpoint blockade [3].

Immunotherapy was recently approved following the impressive benefit of Nivolumab compared to standard chemotherapy in platinum-refractory non-small cell lung cancer (NSCLC) – the CheckMate 017 trial for squamous NSCLC and CheckMate 057 trial for non-squamous NSCLC [4,5]. In CheckMate 017 response rate was 20% with nivolumab versus 9% with docetaxel and the expression of the PD-1 ligand (PD-L1) was neither prognostic nor predictive of benefit, suggesting that in some group of patients there is the need to find additional prognostic features. However, it is important to mention also the CheckMate 026 trial in which Nivolumab was compared to standard chemotherapy in the first-line setting; in that study, immunotherapy was not associated with significantly better outcome compared to standard chemotherapy [6]. Selection criteria for immunotherapy and prognostication might be enriched by comprehensive radiologic characterization.

One option could be histogram analysis, which consists of a group of algorithms which extract numerical parameters from diagnostic images. In the last decade, this quantitative approach has demonstrated a high potential to predict the response to different treatments in different oncological settings, especially in NSCLC [7]. Theoretically, there is no limit to the number of parameters which can be extracted from digital images. In the literature, there is a quite clear distinction between high-throughput approaches (hundreds or thousands of parameters extracted, usually gathered in the name “radiomics”, which lead to highly complex and accurate models) [8] and low-throughput approaches, where a lower number of parameters are analyzed and simpler and probably more robust models are obtained [9]. Among the latter methods, the filtered-histogram showed the greatest diffusion judging by the large number of papers published [10,11]. Notably, the filtered-histogram has been tested on several diagnostic and prognostic tasks for lung cancer management [12], yet its potential in predicting the response to immunotherapy in NSCLC is still unknown.

In this retrospective multicenter study, the filtered-histogram method is tested on pre-treatment computed tomography (CT) of patients treated with Nivolumab after failure of platinum-based chemotherapy to stratify their survival according to CT histogram analysis (CTHA).

2. Materials and methods

2.1. Patients

This retrospective study was approved by the institutional review board of each participating center and was conducted in accordance with the ethical standards of the Declaration of Helsinki.

One hundred and four patients were enrolled from three different centers applying the following inclusion criteria: therapy with Nivolumab after failure of platinum-based schedules (as defined by confirmed imaging progression); availability of pre-treatment contrast-enhanced CT (CECT) performed within 2 months before starting therapy with Nivolumab; no previous radiation therapy on the thorax; follow-up of at least 6 months. Exclusion criteria were: tumor mass <3 cm; ground glass lesion; artefacts on CECT involving the area of interest. The following clinical variables were collected: age, gender, smoking status, Eastern Cooperative Oncology Group (ECOG) score, histology, tumor stage.

2.2. Therapy with Nivolumab

All of the patients received 3 mg Nivolumab per kg every 2 weeks, as second or third line of therapy. Patients were treated until disease progression or discontinuation due to toxicity or other reasons.

2.3. CECT protocol

The CECT protocol was homogeneous in the three participating centers, as follows: a single post-contrast acquisition was performed after injection of 120 mL of iodinated contrast agent (Iomeron 350, Bracco, Milan, Italy), with delay ranging from 75 to 85 s as per standard thoraco-abdominal staging protocol. The CECT was acquired by scanners from three different vendors according to the specific center: Somatom Definition Flash 128 × 2, Somatom Sensation Cardiac 64, Somatom Emotion 6 (Siemens Healthineers).

Tube current ranged between 150 and 200 mA with dose modulation, and tube voltage was 120 kV. Matrix was 512 × 512, reconstruction field of view was tailored to patient size so that pixel dimensions ranged from 0.57 to 1.02 mm. Slice thickness for image analysis included reconstructions at 2–3 mm. Images were reconstructed from the raw data with filtered back-projection using a soft tissue kernel. Images reconstructed with iterative filters were not used because such algorithms were not routinely applied in the three different centers and differed among the three scanners used.

2.4. Follow-up and survival assessment

Clinical evaluation was performed monthly. Follow-up CT was performed every 3 months or in the case of clinical deterioration, as per routine clinical practice. Progression was defined according to iRECIST criteria (modified RECIST guideline for immunotherapy) by experienced radiologists (7–20 years of experience in oncologic imaging); a clinical oncologist dedicated to lung cancer management unified the radiological and clinical data for a comprehensive definition of progression; clinical progression led to immunotherapy discontinuation. Progression-free survival (PFS) and overall survival (OS) were calculated from the date of therapy commencement until progression or death from any cause and were used as outcome indicators; in particular, OS was the primary end point, while PFS was the secondary one. Patients who definitively suspended therapy for toxicity were censored at the date of stopping therapy; patients who temporarily discontinued Nivolumab administration were censured at the date of definitive stop of therapy for any cause.

2.5. Histogram analysis on CECT

Images were transferred from PACS (Picture Archiving and Communication Systems) to an external workstation and were analyzed using the proprietary histogram analysis software TexRAD (TexRAD Ltd, www.texrad.com – part of Feedback Plc). A radiologist with 20 years experience in thoracic imaging drew regions of interest (ROIs) encompassing the tumor across its maximal cross-sectional area in the axial plane as reported in previously published literature [13]. The images reconstructed with a soft-tissue kernel were used for the analysis. Another radiologist with 5 years experience repeated the measurements on 20 randomly selected patients equally distributed between the different centers and scanners to test repeatability.

Double thresholding was applied to exclude pixels below 0 or above 300 Hounsfield Units (HU) in order to exclude cavitations and calcifications [13].

Histogram analysis comprised a filtration-histogram technique, which is described in detail in a previous study [14]. Briefly, a band-pass Laplacian of Gaussian filter (similar to a non-orthogonal wavelet approach) was used to extract and enhance objects of different sizes and intensities within the ROIs. The resulting obtained maps were named by the acronym SSF (*i.e.* Spatial Scale Filter) which was set at 0, 2, 3, 4 and 6 mm, corresponding, respectively, to unfiltered image, fine, medium and coarse “texture” images (Fig. 1). The following first-order parameters were computed from both unfiltered and filtered images: mean, mean of positive pixels, standard deviation, entropy, skewness and kurtosis (peakedness). A detailed analysis of the meaning of these

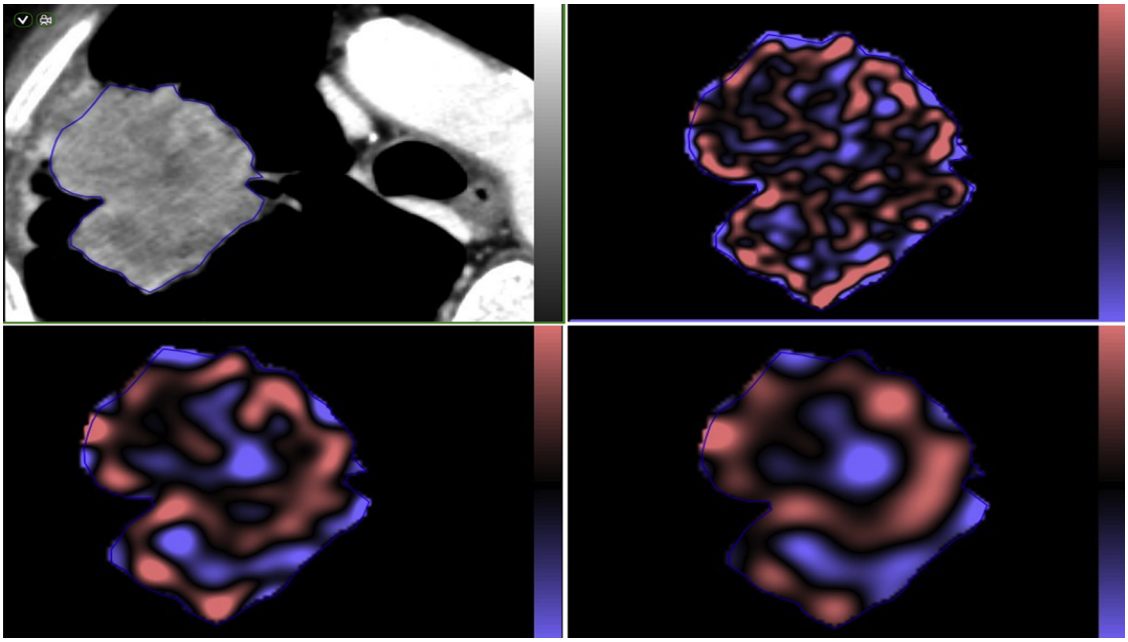

Fig. 1. The figure shows the histogram analysis software. After ROI delineation on the original CT images different filters are applied in order to obtain maps with increasing coarseness.

Table 1
Description of histogram features.

Histogram parameter	description
Mean	Mean density/intensity of all the pixels within the histogram
Mean of positive pixels	Mean density/intensity of image pixels with positive values
Entropy	Metric of image heterogeneity (higher entropy corresponds to more heterogeneous image)
Skewness	Asimmetry of histogram (positive value indicates histogram whose tail is on the right side)
Kurtosis	Peakedness of the histogram (positive values correspond to peaked histograms while negative values to flattened histograms

measurements is provided by Miles et al. [14], see also Table 1.

2.6. Statistical analysis

Relevant histogram features were selected using the Least Absolute Shrinkage and Selection Operator (LASSO) regression analysis method. LASSO can manage survival data and can perform variable selection by fitting a Cox model with 10-fold internal cross-validation to prevent model overfitting. Histogram features were selected according to their prognostic value for OS and PFS, so two different models were obtained. For each of the selected features that maintain prognostic significance, LASSO calculates a coefficient, whose magnitude reflects the strength of the relationship between parameters and outcome. Positive coefficients indicate a positive correlation with the risk of progression or death, whereas negative coefficients suggest a protective effect. External validation was judged to be inadequate because of the small sample size since according to published studies a minimum of 100 events is suggested for an appropriate external validation [15,16].

After calculating the global textural score by the linear combination of the coefficients of the retained variables given by the model and their original value calculated with TexRAD patients were split in two by an optimal cut-off which was calculated by minimizing the p-value of the log-rank test, and from this, the high and low risk groups were identified. A Cox proportional hazards model was built for OS and PFS respectively and hazard ratios (HR) were calculated. Kaplan-meier curves for differences in survival between the high-risk and low-risk groups were plotted.

Repeatability of histogram features between the two operators was tested using the intraclass correlation coefficient (ICC). ICC values less than 0.5 were considered indicative of poor reliability, values between 0.5 and 0.75 indicative of moderate reliability, values between 0.75 and 0.9 indicative of good reliability and values greater than 0.90 indicative of excellent reliability [17].

Statistical analysis was performed in R 3.3.0 and in MedCalc Statistical Software version 18.2.1 (MedCalc Software bvba; http://www.medcalc.org; 2018).

3. Results

3.1. Patients

Baseline characteristics for the 104 patients enrolled in the study are summarized in Table 2. Median follow-up was 13.8 weeks, median OS was 7.3 months (range 0.5–42 months), and median PFS was 3 months (range 0.2–42 months). Sixty-nine patients died during the follow-up, all because of tumor progression. At the time of data extraction, 18 patients were alive and continuing therapy with Nivolumab, while 17 patients were alive, although progression had led to stopping therapy with Nivolumab. Seven patients discontinued therapy because of unacceptable toxicity according to Common Terminology Criteria for Adverse Events (CTCAE) criteria v.4.0.

3.2. Histogram-based model and survival analysis

LASSO selected only one histogram feature related to OS: kurtosis SSF = 4 mm. An inverse correlation was observed between kurtosis (peakedness) and overall survival. The histogram score was computed by multiplying the coefficient obtained with LASSO by feature (kurtosis

Table 2
Baseline characteristics for the 104 patients in this study.

Patient Characteristics	Total No. (%)
Age, median (range), years	67 (43-85)
Gender	35 (33.65%)
Female	69 (66.35%)
Male	
Smoking status	25 (24.03%)
Current	58 (55.77%)
Former (>12 months cessation)	4 (3.85%)
Never	17 (16.35%)
Unknown	
ECOG performance status	63 (60.58%)
0	41 (39.42%)
1	
Histology	75 (72.12%)
Non-squamous	29 (27.88%)
Squamous	
Stage	32 (30.77%)
IIIb	72 (69.23%)
IV	
Duration of treatment, median (range), months	4 (0-26)
Treatment discontinuation	61 (67.78%)
Progression of disease	7 (7.78%)
Toxicity	22 (24.44%)
Other (deterioration of general condition)	
Overall survival, median (range), months	7.3 (0.5-42)
Died	69 (66.35%)
Alive	35 (33.65%)
Progression free survival, median (range), months	3 (0.2-42)

ECOG, Eastern Cooperative Oncology Group.

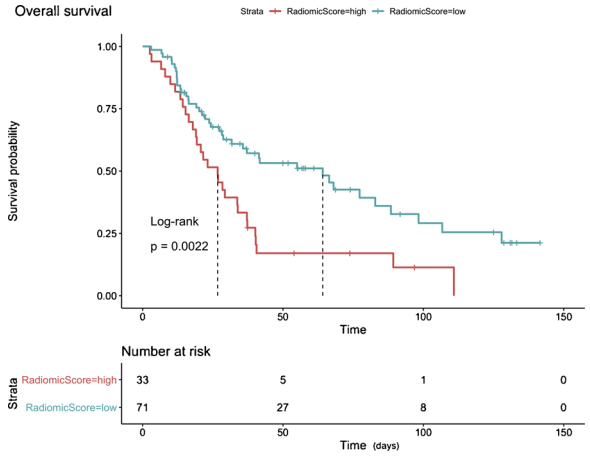

Fig. 2. Kaplan–Meier plots for overall survival (OS). Blue line shows survival of the low score group (RadiomiScore = low), red line shows survival of the high score group (RadiomicScore = high). Reported p-value refers to the log-rank test for differences in overall survival.

SSF = 4 mm) magnitude. The optimal cut-off for histogram score could identify a high-risk group with survival hazard ratio (HR) 0.476 (95%CI 0.29–0.77; p-value of 0.0028, low-risk *vs* high-risk group), as shown by the Kaplan–Meier curves in Fig. 2.

Progression-free survival was related to only one histogram feature: kurtosis SSF = 6 mm. Again, an inverse correlation was observed with PFS. The optimal cut-off for histogram score could identify two groups with difference in PFS (HR 0.556 for low-risk *vs* high-risk group, 95%CI 0.36–0.86; p-value 0.0088), as displayed by the Kaplan–Meier curves in Fig. 3.

The intraclass correlation coefficient (ICC) for kurtosis SSF = 4 mm was 0.89 (95%CI 0.71–0.96), and for kurtosis SSF = 6 mm, the ICC was 0.83 (95%CI 0.57–0.93) indicating good reliability of the results.

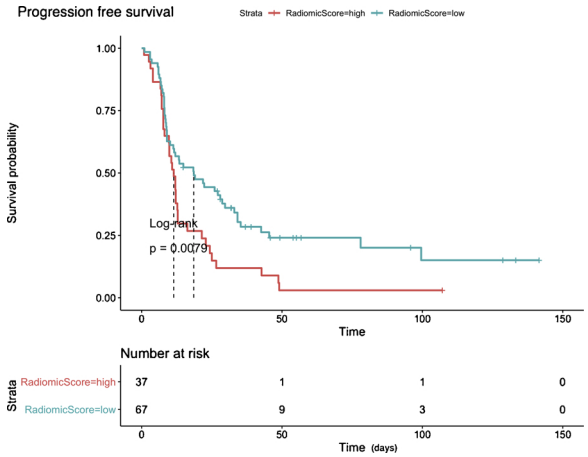

Fig. 3. Kaplan–Meier plots for progression-free survival (PFS). Blue line shows survival of the low score group (RadiomicScore = low), red line shows survival of the high score group (RadiomicScore = high). Reported p-value refers to the log-rank test for differences in progression-free survival.

4. Discussion

Immunotherapy represents the most advanced medical treatment for NSCLC, with unprecedented potential for development. This retrospective study investigated CT histogram analysis (CTHA) for prognostic stratification of NSCLC patients treated with Nivolumab. We showed that CTHA using the filtration-histogram technique could stratify both OS and PFS according to kurtosis with SSF = 4 mm or SSF = 6 mm, respectively.

The filtration-histogram technique of CTHA was proposed by Miles et al [14]. It highlights relatively hyperdense (higher contrast-enhancement) areas with a predefined size-scale and suppresses relatively hypodense (lower contrast-enhancement) areas with the same size-scale within the selected ROI, thus indicating the tumor. Compared to other texture analysis methods and radiomics approaches, it produces a relatively low number of parameters which reflect quite intuitive image characteristics [9]. Furthermore, the initial step of image filtration renders the parameters less sensitive to intrinsic image noise that largely varies according to acquisition parameters and different scanners [18].

This multicenter retrospective study demonstrated that histogram features are correlated with OS and PFS in an homogeneous cohort of patients affected by solid tumors treated with Nivolumab after failure of platinum-based chemotherapy. As mentioned above, the number of patients was not sufficiently high to allow an external validation to be performed; however, the LASSO algorithm is strictly selective and 10-fold cross-validation used to extract the prognostic model increased the robustness of this method and reduced the probability of overfitting.

For both OS and PFS, the feature kurtosis on coarse “texture” (SSF = 4 mm and SSF = 6 mm, respectively) had a prognostic value. This parameter represents the peakedness of the histogram of the image and, on histogram maps, is inversely correlated with the number of highlighted objects but positively related with the intensity variation of objects highlighted by the image filter [14]. This could imply that lesions with more homogeneous enhancement (lower intensity variation among highlighted objects) are less responsive to immunotherapy. This result seems to be supported by the results obtained by another paper recently published by our group, in which kurtosis at different spatial scales seems to be inversely correlated with PFS in patients with lung adenocarcinoma treated with tyrosine kinase inhibitors (TKIs) [19]. Based on these two preliminary observations, kurtosis seems a good candidate for in vivo stratification of tumor responsiveness to different therapies, and perhaps aggressiveness; however, in the abovementioned study, kurtosis correlated with just PFS and not with OS and should be

considered to be a predictive rather than a prognostic factor related to TKI therapy.

Another study recently published by Sun et al. [20] makes the interpretation of our results more controversial. In a heterogeneous group of several types of tumor treated with immunotherapy, Sun et al. aimed to find a correlation between radiomics and lymphocitary infiltrates, an entity which is positively associated with survival. The results showed that a radiomic signature for homogeneous tumors (MOSCATO trial) was linked to high levels of CD8 within the tumors and correlated with better overall survival. On the other hand, our results are in line with Tang et al. who recently investigated NSCLC treated with standard chemotherapy and reported a radiomic signature consistent with high tumor heterogeneity, which was associated with CD3+ cell count and thus with better survival [21].

To the best of our knowledge, this is the first study which tested quantitative CT analysis in solid primary lung cancer treated with Nivolumab. If confirmed on external datasets, the results of this study could help clinicians make clinical decisions, providing a pre-treatment probability of response which could help to interpret later changes, which may be unexpected, and therefore could add diagnostic information for early clinical decisions on immunotherapy maintenance or discontinuation.

This study has several limitations. First, the retrospective shape implied a non-systematic collection of clinical data, thus resulting in potential differences in contrast agent dynamics. The second limitation was the absence of an external validation cohort, which was not possible because of the small number in this population. Third, the analysis was performed on a single slice, therefore this may not represent the whole tumor heterogeneity; also, voxels were not resampled among the different scanners and studies in order to obtain a constant sample size; however, previous studies showed that parameters describing histogram morphology (such as kurtosis and skewness) are robust and have a low variability across images with different voxel size even in multicentric studies [22,23]. Fourth, we have no data about lymphocyte pattern of tissue biopsies and this represents a missed opportunity to provide a more comprehensive insight into this still unclear field.

5. Conclusion

In conclusion, the present study showed that the outcome of NSCLC treated with immunotherapy can be assessed by baseline CTHA for prognostication of OS and PFS. We plan to perform further studies to analyze these preliminary findings with the aim of investigating CTHA in the complex management of NSCLC under immunotherapy.

Disclosure paragraph

The authors state that this work has not received any funding and the study was conducted in compliance with Ethical Standards (declaration of Helsinki). One of the authors (Balaji Ganeshan) is a director, part-time employee, and shareholder of Feedback Plc (Cambridge, England, UK), company that develops and markets TexRAD texture analysis algorithm described in this manuscript.

Acknowledgements and Conflict of Interests

One of the authors (Balaji Ganeshan) is a director, part-time employee, and shareholder of Feedback Plc (Cambridge, England, UK), company that develops and markets TexRAD texture analysis algorithm described in this manuscript.

References

[1] Global Burden of Disease Cancer Collaboration, C. Fitzmaurice, C. Allen, R.M. Barber, L. Barregard, Z.A. Bhutta, H. Brenner, D.J. Dicker, O. Chimed-Orchir, R. Dandona, L. Dandona, T. Fleming, M.H. Forouzanfar, J. Hancock, R.J. Hay, R. Hunter-Merrill, C. Huynh, H.D. Hosgood, C.O. Johnson, J.B. Jonas, J. Khubchandani, G.A. Kumar, M. Kutz, Q. Lan, H.J. Larson, X. Liang, S.S. Lim, A.D. Lopez, M.F. MacIntyre, L. Marczak, N. Marquez, A.H. Mokdad, C. Pinho, F. Pourmalek, J.A. Salomon, J.R. Sanabria, L. Sandar, B. Sartorius, S.M. Schwartz, K.A. Shackelford, K. Shibuya, J. Stanaway, C. Steiner, J. Sun, K. Takahashi, S.E. Vollset, T. Vos, J.A. Wagner, H. Wang, R. Westerman, H. Zeeb, L. Zoeckler, F. Abd-Allah, M.B. Ahmed, S. Alabed, N.K. Alam, S.F. Aldhahri, G. Alem, M.A. Alemayohu, R. Ali, R. Al-Raddadi, A. Amare, Y. Amoako, A. Artaman, H. Asayesh, N. Atnafu, A. Awasthi, H.B. Saleem, A. Barac, N. Bedi, I. Bensenor, A. Berhane, E. Bernabé, B. Betsu, A. Binagwaho, D. Boneya, I. Campos-Nonato, C. Castañeda-Orjuela, F. Catalá-López, P. Chiang, C. Chibueze, A. Chitheer, J.-Y. Choi, B. Cowie, S. Damtew, J. das Neves, S. Dey, S. Dharmaratne, P. Dhillon, E. Ding, T. Driscoll, D. Ekwueme, A.Y. Endries, M. Farvid, F. Farzadfar, J. Fernandes, F. Fischer, T.T. G/Hiwot, A. Gebru, S. Gopalani, A. Hailu, M. Horino, N. Horita, A. Husseini, I. Huybrechts, M. Inoue, F. Islami, M. Jakovljevic, S. James, M. Javanbakht, S.H. Jee, A. Kasaeian, M.S. Kedir, Y.S. Khader, Y.-H. Khang, D. Kim, J. Leigh, S. Linn, R. Lunevicius, H.M.A. El Razek, R. Malekzadeh, D.C. Malta, W. Marcenes, D. Markos, Y.A. Melaku, K.G. Meles, W. Mendoza, D.T. Mengiste, T.J. Meretoja, T.R. Miller, K.A. Mohammad, A. Mohammadi, S. Mohammed, M. Moradi-Lakeh, G. Nagel, D. Nand, Q. Le Nguyen, S. Nolte, F.A. Ogbo, K.E. Oladimeji, E. Oren, M. Pa, E.-K. Park, D.M. Pereira, D. Plass, M. Qorbani, A. Radfar, A. Rafay, M. Rahman, S.M. Rana, K. Søreide, M. Satpathy, M. Sawhney, S.G. Sepanlou, M.A. Shaikh, J. She, I. Shiue, H.R. Shore, M.G. Shrime, S. So, S. Soneji, V. Stathopoulou, K. Stroumpoulis, M.B. Sufiyan, B.L. Sykes, R. Tabarés-Seisdedos, F. Tadese, B.A. Tedla, G.A. Tessema, J.S. Thakur, B.X. Tran, K.N. Ukwaja, B.S.C. Uzochukwu, V.V. Vlassov, E. Weiderpass, M. Wubshet Terefe, H.G. Yebyo, H.H. Yimam, N. Yonemoto, M.Z. Younis, C. Yu, Z. Zaidi, M.E.S. Zaki, Z.M. Zenebe, C.J.L. Murray, M. Naghavi, Global, regional, and national Cancer incidence, mortality, years of life lost, years lived with disability, and disability-adjusted life-years for 32 Cancer groups, 1990 to 2015: a systematic analysis for the global burden of disease study, JAMA Oncol. 3 (2017) 524–548, https://doi.org/10.1001/jamaoncol.2016.5688.

[2] S. Muenst, H. Läubli, S.D. Soysal, A. Zippelius, A. Tzankov, S. Hoeller, The immune system and cancer evasion strategies: therapeutic concepts, J. Intern. Med. 279 (2016) 541–562, https://doi.org/10.1111/joim.12470.

[3] M. Reck, K.F. Rabe, Precision diagnosis and treatment for advanced non–small-cell lung Cancer, N. Engl. J. Med. 377 (2017) 849–861, https://doi.org/10.1056/NEJMra1703413.

[4] J. Brahmer, K.L. Reckamp, P. Baas, L. Crinò, W.E.E. Eberhardt, E. Poddubskaya, S. Antonia, A. Pluzanski, E.E. Vokes, E. Holgado, D. Waterhouse, N. Ready, J. Gainor, O. Arén Frontera, L. Havel, M. Steins, M.C. Garassino, J.G. Aerts, M. Domine, L. Paz-Ares, M. Reck, C. Baudelet, C.T. Harbison, B. Lestini, D.R. Spigel, Nivolumab versus docetaxel in advanced squamous-cell non-small-cell lung Cancer, N. Engl. J. Med. 373 (2015) 123–135, https://doi.org/10.1056/NEJMoa1504627.

[5] H. Borghaei, L. Paz-Ares, L. Horn, D.R. Spigel, M. Steins, N.E. Ready, L.Q. Chow, E.E. Vokes, E. Felip, E. Holgado, F. Barlesi, M. Kohlhäufl, O. Arrieta, M.A. Burgio, J. Fayette, H. Lena, E. Poddubskaya, D.E. Gerber, S.N. Gettinger, C.M. Rudin, N. Rizvi, L. Crinò, G.R. Blumenschein, S.J. Antonia, C. Dorange, C.T. Harbison, F. Graf Finckenstein, J.R. Brahmer, Nivolumab versus docetaxel in advanced non-squamous non-small-cell lung Cancer, N. Engl. J. Med. 373 (2015) 1627–1639, https://doi.org/10.1056/NEJMoa1507643.

[6] D.P. Carbone, M. Reck, L. Paz-Ares, B. Creelan, L. Horn, M. Steins, E. Felip, M.M. van den Heuvel, T.-E. Ciuleanu, F. Badin, N. Ready, T.J.N. Hiltermann, S. Nair, R. Juergens, S. Peters, E. Minenza, J.M. Wrangle, D. Rodriguez-Abreu, H. Borghaei, G.R. Blumenschein, L.C. Villaruz, L. Havel, J. Krejci, J. Corral Jaime, H. Chang, W.J. Geese, P. Bhagavatheeswaran, A.C. Chen, M.A. Socinski, CheckMate 026 investigators, first-line nivolumab in stage IV or recurrent non-small-cell lung Cancer, N. Engl. J. Med. 376 (2017) 2415–2426, https://doi.org/10.1056/NEJMoa1613493.

[7] I. Phillips, M. Ajaz, V. Ezhil, V. Prakash, S. Alobaidli, S.J. McQuaid, C. South, J. Scuffham, A. Nisbet, P. Evans, Clinical applications of textural analysis in non-small cell lung cancer, Br. J. Radiol. 91 (2018) 20170267, , https://doi.org/10.1259/bjr.20170267.

[8] S. Rizzo, F. Botta, S. Raimondi, D. Origgi, C. Fanciullo, A.G. Morganti, M. Bellomi, Radiomics: the facts and the challenges of image analysis, Eur. Radiol. Exp. 2 (2018) 36, https://doi.org/10.1186/s41747-018-0068-z.

[9] M.G. Lubner, A.D. Smith, K. Sandrasegaran, D.V. Sahani, P.J. Pickhardt, CT texture analysis: definitions, applications, biologic correlates, and challenges, RadioGraphics. 37 (2017) 1483–1503, https://doi.org/10.1148/rg.2017170056.

[10] C. Durot, S. Mulé, P. Soyer, A. Marchal, F. Grange, C. Hoeffel, Metastatic melanoma: pretreatment contrast-enhanced CT texture parameters as predictive biomarkers of survival in patients treated with pembrolizumab, Eur. Radiol. 29 (6) (2019) 3183–3191, https://doi.org/10.1007/s00330-018-5933-x.

[11] L. Brenet Defour, S. Mulé, A. Tenenhaus, T. Piardi, D. Sommacale, C. Hoeffel, G. Thiéfin, Hepatocellular carcinoma: CT texture analysis as a predictor of survival after surgical resection, Eur. Radiol. 29 (2019) 1231–1239, https://doi.org/10.1007/s00330-018-5679-5.

[12] S.Y. Ahn, C.M. Park, S.J. Park, H.J. Kim, C. Song, S.M. Lee, H.P. McAdams, J.M. Goo, Prognostic value of computed tomography texture features in non–Small cell lung cancers treated with definitive concomitant chemoradiotherapy, Invest. Radiol. 50 (2015) 719–725, https://doi.org/10.1097/RLI.0000000000000174.

[13] K.A. Miles, How to use CT texture analysis for prognostication of non-small cell lung cancer, Cancer Imaging 16 (2016), https://doi.org/10.1186/s40644-016-0065-5.

[14] K.A. Miles, B. Ganeshan, M.P. Hayball, CT texture analysis using the filtration-histogram method: what do the measurements mean? Cancer Imag. off. Publ. Int. Cancer Imag. Soc. 13 (2013) 400–406, https://doi.org/10.1102/1470-7330.2013.

9045.
[15] G.S. Collins, E.O. Ogundimu, D.G. Altman, Sample size considerations for the external validation of a multivariable prognostic model: a resampling study, Stat. Med. 35 (2016) 214–226, https://doi.org/10.1002/sim.6787.
[16] E.W. Steyerberg, Validation in prediction research: the waste by data splitting, J. Clin. Epidemiol. 103 (2018) 131–133, https://doi.org/10.1016/j.jclinepi.2018.07.010.
[17] T.K. Koo, M.Y. Li, A guideline of selecting and reporting intraclass correlation coefficients for reliability research, J. Chiropr. Med. 15 (2016) 155–163, https://doi.org/10.1016/j.jcm.2016.02.012.
[18] A. Midya, J. Chakraborty, M. Gönen, R.K.G. Do, A.L. Simpson, Influence of CT acquisition and reconstruction parameters on radiomic feature reproducibility, J. Med. Imag. Bellingham Wash. 5 (2018) 011020, , https://doi.org/10.1117/1.JMI.5.1.011020.
[19] M. Ravanelli, G.M. Agazzi, B. Ganeshan, E. Roca, E. Tononcelli, V. Bettoni, A. Caprioli, A. Borghesi, A. Berruti, R. Maroldi, D. Farina, CT texture analysis as predictive factor in metastatic lung adenocarcinoma treated with tyrosine kinase inhibitors (TKIs), Eur. J. Radiol. 109 (2018) 130–135, https://doi.org/10.1016/j.ejrad.2018.10.016.
[20] R. Sun, E.J. Limkin, M. Vakalopoulou, L. Dercle, S. Champiat, S.R. Han, L. Verlingue, D. Brandao, A. Lancia, S. Ammari, A. Hollebecque, J.-Y. Scoazec, A. Marabelle, C. Massard, J.-C. Soria, C. Robert, N. Paragios, E. Deutsch, C. Ferté, A radiomics approach to assess tumour-infiltrating CD8 cells and response to anti-PD-1 or anti-PD-L1 immunotherapy: an imaging biomarker, retrospective multicohort study, Lancet Oncol. 19 (2018) 1180–1191, https://doi.org/10.1016/S1470-2045(18)30413-3.
[21] C. Tang, B. Hobbs, A. Amer, X. Li, C. Behrens, J.R. Canales, E.P. Cuentas, P. Villalobos, D. Fried, J.Y. Chang, D.S. Hong, J.W. Welsh, B. Sepesi, L. Court, I.I. Wistuba, E.J. Koay, Development of an immune-pathology informed radiomics model for non-small cell lung Cancer, Sci. Rep. 8 (2018) 1922, https://doi.org/10.1038/s41598-018-20471-5.
[22] A. Traverso, L. Wee, A. Dekker, R. Gillies, Repeatability and reproducibility of radiomic features: a systematic review, Int. J. Radiat. Oncol. Biol. Phys. 102 (2018) 1143–1158, https://doi.org/10.1016/j.ijrobp.2018.05.053.
[23] Radiomics of Lung Nodules: A Multi-Institutional Study of Robustness and Agreement of Quantitative Imaging Features, Tomography 2 (2016) 430–437, https://doi.org/10.18383/j.tom.2016.00235.